# Receiver notching in a linear V(z) near-surface medium

Dan Cieslewicz and Don C. Lawton


## ABSTRACT

Receiver notching occurs when a seismic reflection interferes destructively with its multiple off the surface. While common in marine seismic data, receiver notching does not occur in most land data, as geophones are usually placed at the surface where the interference is constructive. However, data from buried geophones, such as those from the Blackfoot III experiment, may be expected to contain receiver notches, which can adversely affect data quality. Receiver notching was investigated with computer simulations of a broadband Ricker wavelet traveling through a linear V(z) medium (as a first approximation of the true near surface) and interfering with itself after reflecting off a free surface. The effect of the interference on wavelet amplitude was also studied. Amplitudes were also investigated separately with an I(z) impedance model. The simulations indicate receiver notching occurs for depths of over one meter for near-surface velocity values typical of the Blackfoot III area. Interference decreases amplitudes to a minimum of about 27% of surface values, regardless of the velocity gradient. Below this depth, amplitudes increase to the value of the incident wavelet at a rate proportional to the average velocity of the media and the velocity gradient. The notches asymptotically approach zero frequency at greater depths at a rate inversely proportional to average velocity and velocity gradient. Additional high-frequency notches appear at depth and follow the same pattern, resulting in an often intricate pattern of notching at a function of depth. The impedance model amplitude simulations indicated that a medium of decreasing impedance would act as a natural signal amplifier, resulting in higher reflection amplitudes for shallower geophones. In several examples, the frequency spectra of reflections recorded by the Blackfoot III buried geophones contained notches not present in the surface geophone data. The converted-wave data contained more depth-dependent notches than the compressional-wave data, as predicted by the simulations. The amplitude simulations based on the impedance model strongly agreed with the real data, while the amplitude simulations from wavelet interference had little agreement. The study indicates that receiver notching occurs in buried geophones, and that the sharp impedance gradient of the near surface amplifies reflections, resulting in higher average absolute amplitudes for shallower geophones.


## INTRODUCTION

Notching is a well-recognized phenomenon that can adversely affect the quality of seismic data. Notching occurs when two or more seismic pulses (such as a primary reflection and its multiples) superimpose and destructively interfere at certain frequencies. The interference causes the amplitude spectrum of the recorded data to have one or more pronounced gaps or notches at discrete frequencies (example, Figure 1). This causes distortions in the shape of the recorded wavelet, which can lead to difficulties in seismic interpretation in cases where reflection character is important.

Seismic waves can become superimposed and cause frequency notching in many ways. Source ghosting, for example, is a type of multiple that occurs when the primary pulse is superimposed with its reflection from the water surface (in marine surveys) or the water table (in land surveys). This will cause angle-dependent frequency notching and pronounced directionality of the source signal (Waters, 1987). In land seismic surveys, the source ghost problem is controlled partially by locating the source charges at a constant depth beneath the multiple-generating water table, which results in a fairly consistent source ghosting pattern (and therefore reflection character). Notching can also occur due to seismic wave interference at the location of the receiver, known as receiver notching. This occurs in marine seismic surveys, when an incident primary reflection interferes with a reflection from the surface of the water. Receiver notching is reduced by locating the receivers at 10-15 meters below the water surface, which causes the interference to be constructive in the seismic data range of 25 to 40 Hertz.

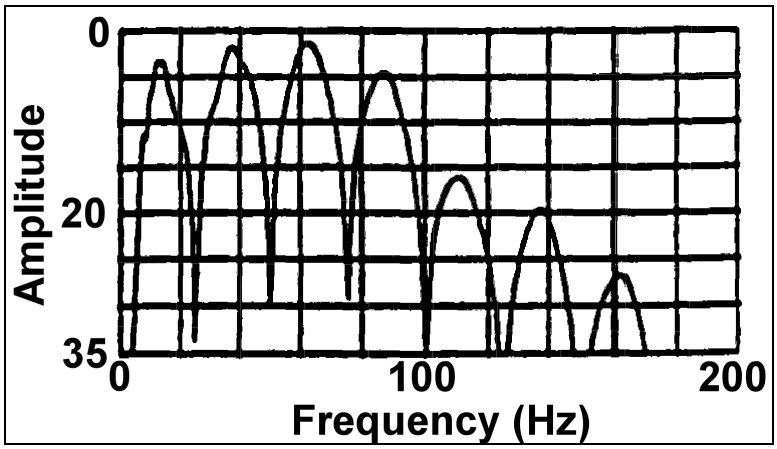


Figure 1. Frequency spectra of raw hydrophone data from a marine seismic survey. The pronounced notches are due to the incident primary reflection interfering with its reflection from the water surface (from Sheriff and Geldart, 1995).

In most land surveys, receiver notching due to surface reflections does not occur because geophones are normally planted directly on the surface or in shallow holes. The surface has a reflection coefficient of nearly -1, and so the incident and reflected wavelets interfere constructively at the interface. This causes a beneficial doubling of the reflection amplitudes compared to their subsurface amplitudes, which is termed the free surface effect. Data from buried geophones will not benefit from the signal-enhancing free surface effect, and may be degraded by receiver notching.

A straightforward application of the Zoeppritz equations demonstrates that average reflection amplitudes recorded by buried geophones are a function of the near-surface impedance gradient. This effect is entirely independent from wavelet interference.

This paper investigates reflection amplitudes and receiver notching that might be expected for buried geophones through simulations of a model wavelet propagating through a linear V(z) near-surface medium that is bounded on one side by a free surface. The amplitude effect due to variations in near surface impedance is investigated separately with an I(z) near-surface impedance model based on a linear V(z) and $\rho(z)$. Results are compared to data from the Blackfoot III buried geophone

experiment, where reflection amplitudes from the buried geophones were found to be significantly lower than those recorded by the surface geophones.

## SIMULATIONS

All simulations for this study were performed using the Matlab computer programming language on a Sun/Sparc workstation.

### Design of the Model Near Surface

Receiver notches in marine surveys are relatively predictable, as the velocity of water is a known constant. Combining hydrophone and geophone data can mitigate these notches, which tend to have opposite receiver notching patterns (Barr and Sanders, 1989). For land surveys, however, the near surface can have a complex vertical and lateral velocity structure that is usually not known to any great detail. However, near-surface seismic studies have found that across the first 20 or so meters, the P-wave velocity of overburden sediments can increase from subsonic values to over six times the speed of sound in air (Miller and Xia, 1998). The velocity increase is due to the water table and the bedrock surface. To study receiver notching in land surveys, then, a constant-velocity near-surface model is not a good approximation.

For this study, a more appropriate linear V(z) model is used as a first approximation of the true near-surface layer. Values chosen for the synthetic models are based on linear gradients between vertical velocity measurements of the near-surface layer in the Blackfoot area (Cieslewicz and Lawton, 1998b). Because almost no geologic feature can be described as truly linear, least of all the near-surface layer, the results are not expected to be an accurate predictor of expected receiver notches. Instead, they will be used to identify general patterns of receiver notching over a range of receiver depths and near-surface velocity gradients. If present in the buried geophone data, these general patterns will indicate that receiver notching can be a factor in the quality of buried geophone data.

For reflection amplitude simulations, an I(z) impedance model is derived by multiplying a plausible linear $\rho(z)$ model with the V(z) model.

### Construction of Model Source Wavelet

A 30-Hertz dominant frequency Ricker wavelet served as the model source wavelet to simulate a broadband reflection. This function is the second derivative of the Gaussian error function (the classic bell curve), and is expressed analytically as

$$r(t) = (1 - 2\pi^2 \nu_M^2 t^2) e^{-\pi^2 \nu_M^2 t^2},$$

where r(t) is a Ricker wavelet with a mean (or "dominant") frequency of $\nu_{mean} = (2/\pi^2)\nu_M$.



Contents

Figure 2(a) shows the time-domain representation of the source wavelet, and Figure 2(b) shows its frequency spectrum. The frequency spectrum shows that most energy in the wavelet is contained in the 15 to 45 Hertz range and tapers off more sharply at lower frequencies than higher frequencies. These frequency characteristics are typical for most pre-whitened seismic reflection data.

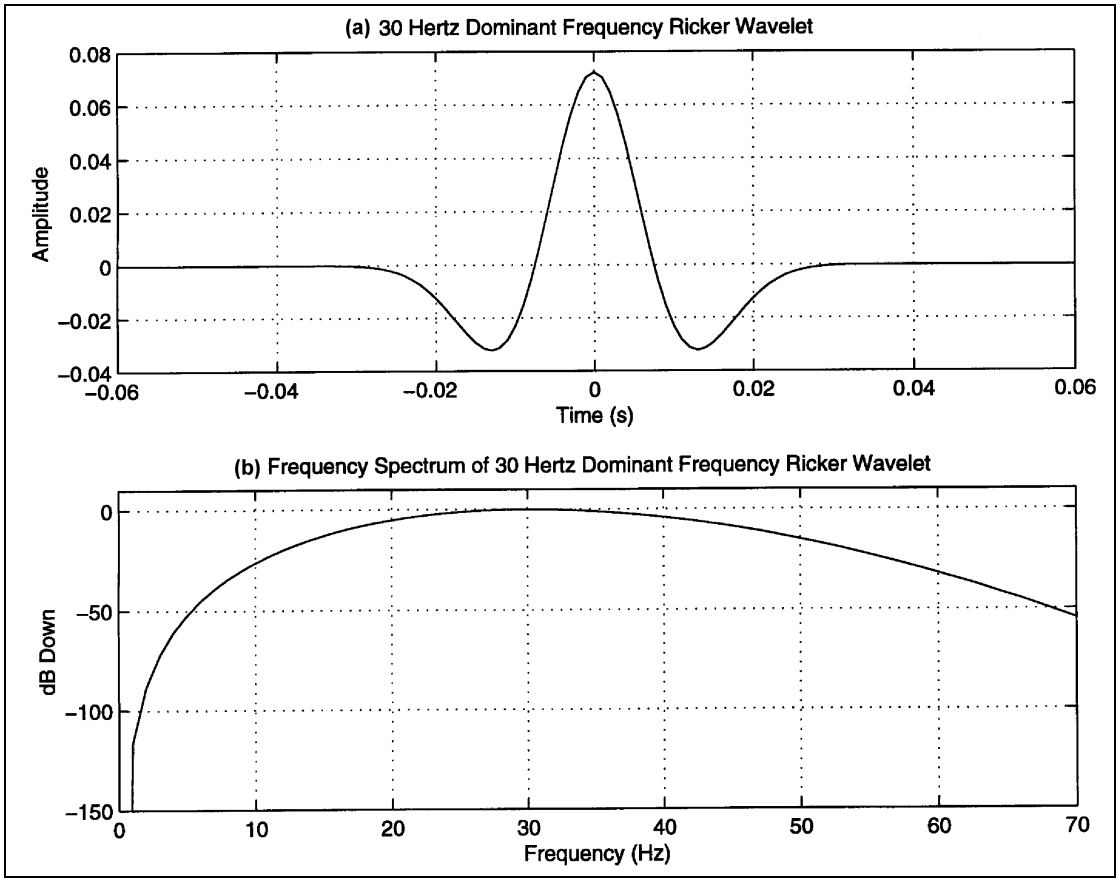


Figure 2. The (a) time and (b) frequency domain plots of the 30-Hertz Ricker wavelet used as the model source wavelet.

## Numerical Simulation of Propagating Wavelet

All simulations were performed with a Matlab function written for this study. The function allows the user to select the dominant frequency of the source Ricker wavelet, the receiver depths at which to look for notches, the time vector over which to "record" data, and the seismic velocities at the depth of the deepest geophone and at surface.

The function depth-steps the Ricker wavelet through each of the designated receiver depths, from the deepest to the shallowest, using the velocity gradient together with the appropriate kinematic equations. This is the "incident" wave field. It then performs the identical procedure, but starting from the shallowest geophone depth and propagating the wavelet downward (practically, the only difference is the presence of a minus sign in the propagating equation), to determine the "reflected" wave field. The phase of the incident and reflected wavelets is identical to simulate a wave that has reflected off a surface with reflection coefficient of -1 as recorded by a



Contents

velocity-sensitive receiver (the geophones). Though the wave reverses polarity upon reflection, it is traveling in the opposite direction as the incident wave. Since geophones cannot distinguish between a push from below and a pull from above, the reflected wave would be recorded with the same polarity as the incident. The total wave field recorded is found by simply summing the incident and reflected wave fields.

*Example*

The Matlab function plots the incident, reflected and total wave fields as wiggle traces. Figure 3 shows an example of a 30-Hertz Ricker wavelet propagating vertically upwards through the top 18m of a near-surface layer whose velocity decreases linearly from 3100 m/s to 300 m/s. The near surface model might represent an extreme situation of glacial till containing the water table overlying relatively unweathered sandstone. This simulation is a common shot gather consisting of 76 buried geophones recording data at a depth increment of 0.25 m. At depths below 9m or so, velocities are still high and the wavelet appears to arrive at each geophone nearly simultaneously. At shallower depths, the wavelet arrives at each geophone with a successively greater lag time. This plot represents the incident wave field. Figure 4 shows the same wavelet, having reflected off the free surface at 0m, propagating to greater depths. This represents the reflected wave field. Figure 5 shows the sum of the incident and reflected wave fields. This is the total wave field.

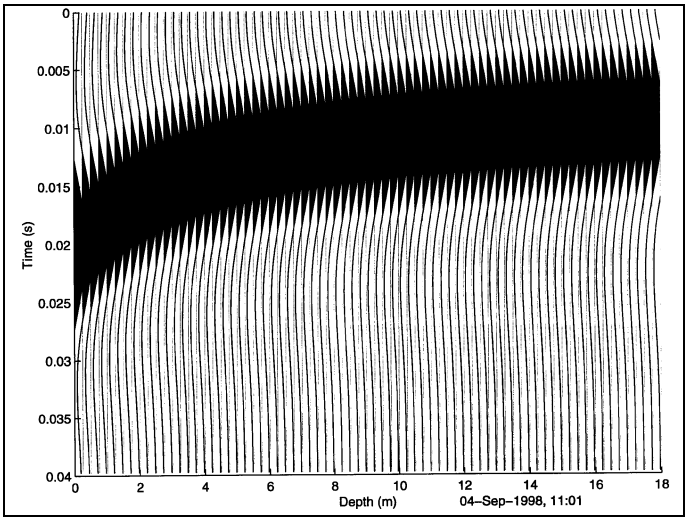


Figure 3. Incident 30-Hertz Ricker wavelet in a linear V(z) medium.



Contents

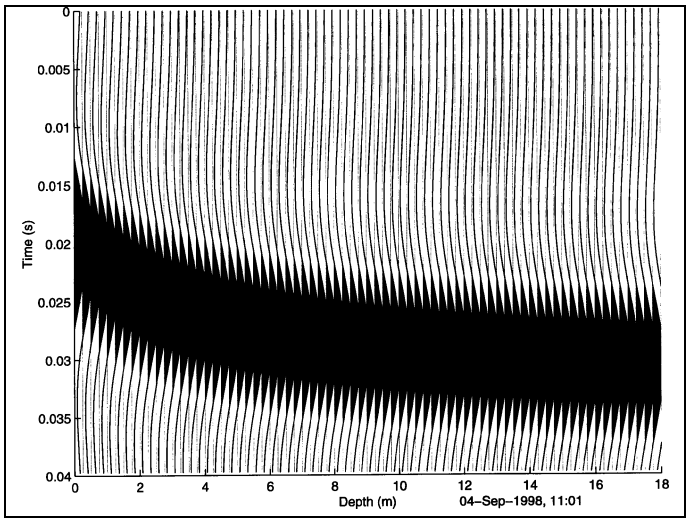


Figure 4. Reflected 30-Hertz Ricker wavelet, which is the same as the incident wavelet after reflection off the free surface at 0m.

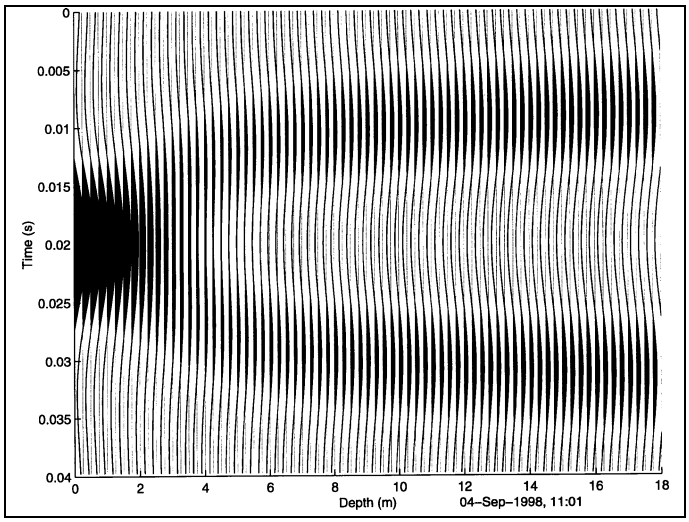


Figure 5. Total wavefield (incident+reflected), which is detected by the geophones.

The shape of the incident, reflected and total wave field for a given time may be viewed in the depth domain. Figure 6 shows a "snapshot" of what each field looks like just before the Ricker wavelet peak reaches the surface (t=0.018s). Because of the severe velocity gradient, the incident and reflected wavelets are stretched greatly at depths below about 6m, and do not resemble the Ricker wavelet as recorded in the (linear) time domain (Figure 1a). The total wave field is twice the amplitude of the incident at a depth of 0m, due to the free surface effect. At depths between about 2m and 17m, the absolute amplitude of the total wave field is less than that of either the incident or reflected wave fields, and is zero at about 7 meters depth. This indicates that destructive interference is occurring, which suggests that geophones buried at depths between 2 and 17 meters could be expected to have poorer signal-to-noise ratios than geophones at other depths. Note also that the shape of the total wave field is different from both the incident and reflected wavelet, indicating that wavelet distortion has occurred.

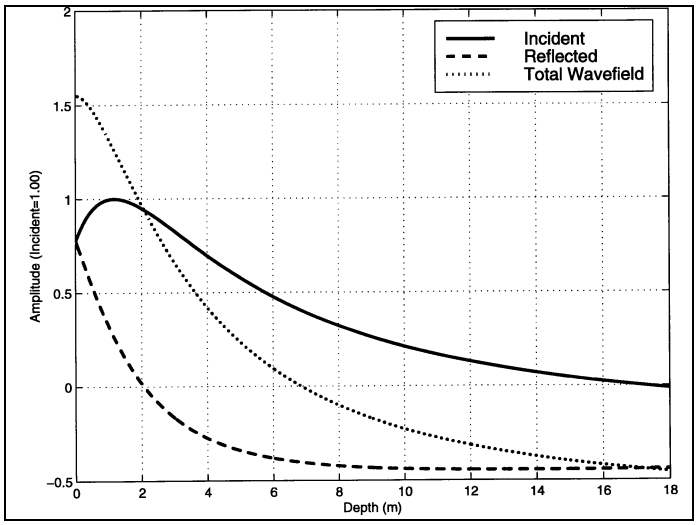


Figure 6. The depth-domain appearance of the incident, reflected and total wave fields for a 30-Hertz dominant frequency Ricker wavelet at t=0.018s. Near-surface velocity is linear: $V_0$=300m/s, $V_{18}$=3100. Interference is constructive to a depth of 2 meters, and mostly destructive at greater depths.

## Receiver Notching

Depth-dependent receiver notches are investigated by taking the Fourier spectrum at each depth of the total wavefield. The patterns of receiver notches were rather intricate, and not exhibited well on a two-dimensional line plot. To display the data in all three dimensions of depth, frequency and amplitude, the data were plotted as grayscale contours. Figure 7 is an example of such a plot for the velocity gradient discussed in the previous section. The plot reveals a 100-Hertz receiver notch emerging at a depth of one meter below surface. With increasing depth, the notch rapidly moves to lower frequencies, reaching about 27 Hertz at 18 meters depth. An additional high-frequency notch emerges at 6m depth and follows the same pattern, declining to about 75 Hertz at 18 meters depth. This plot indicates that a geophone located between 4 and 18 meters depth in this medium would have a notch in the dominant frequency range for seismic data.

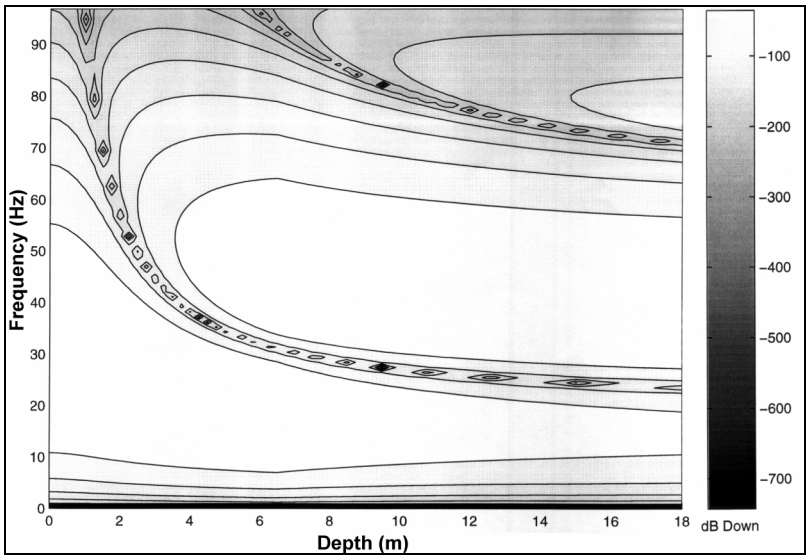


Figure 7. Grayscale contour plot of frequency spectrum of a 30-Hertz Ricker wavelet reflecting in a steep-gradient ($V_0$=300 m/s, $V_{18}$=3100 m/s) linear V(z) medium bounded by a free surface. The contours represent decibels down from the maximum amplitude.

Figure 8 shows the same plot for a shallower ($V_0$=300 m/s, $V_{18}$=2200 m/s) velocity gradient, that is might represent glacial overburden overlying weathered bedrock. These are more typical velocity values for the Blackfoot area. The high-frequency notch appears at one meter depth as before, but declines to 20-Hertz frequency at 18 meters depth. Two additional notches join the first at depth increases. A medium with an even shallower velocity gradient ($V_0$=300 m/s, $V_{18}$=900 m/s) may represent an overburden layer composed entirely of glacial till with a deep water table. Its pattern of expected receiver notches appears in Figure 9. At this gradient, 6 notches have appeared at the 18 meter depth, and almost every depth contains one or more notches in the dominant bandwidth of the source Ricker wavelet.

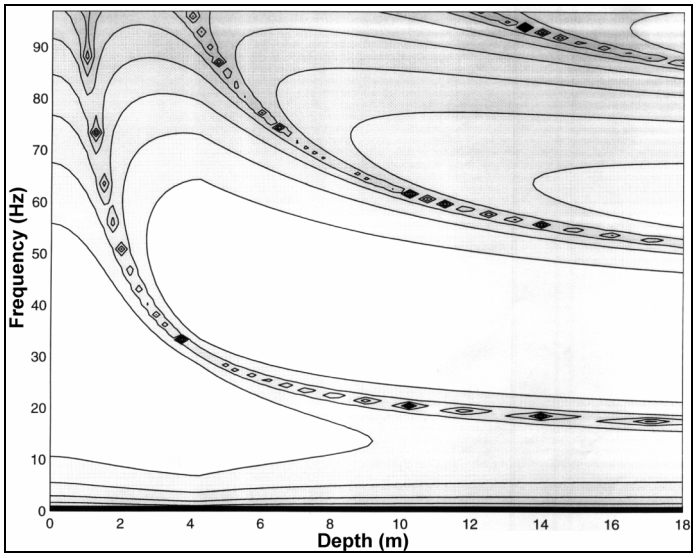


Figure 8. Same as Figure 7 but for a shallower velocity gradient ($V_0$=300 m/s, $V_{18}$=2200 m/s). Colourbar scheme same as Figure 7.



Contents

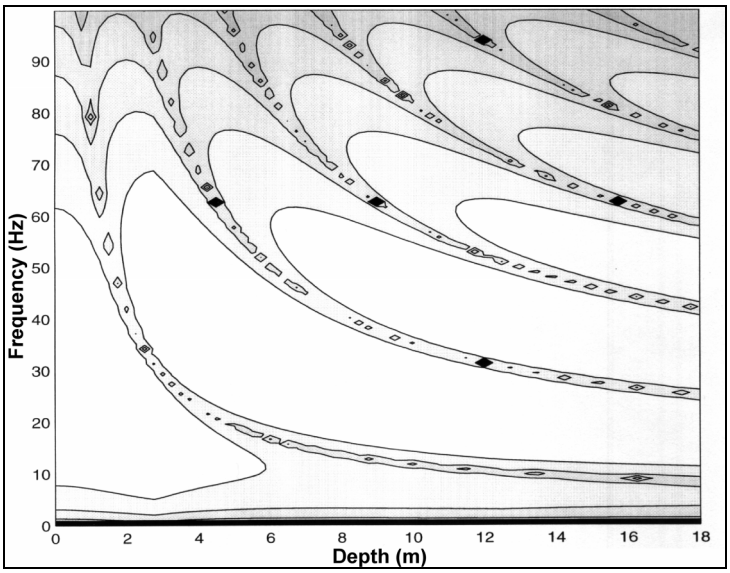


Figure 9. Same as Figure 7 but for $V_0$=300 m/s, $V_{18}$=900 m/s.

Figure 10 shows a contoured plot of a constant velocity medium (V=900 m/s), for comparison purposes, which represents the average velocity of the top 18 meters of the surface layer in the Blackfoot III area as determined from uphole shot times. Notching patterns for this medium are similar to those with a linear V(z), except that the notches asymptotically approach each axis at about the same rate, giving the plot greater symmetry.

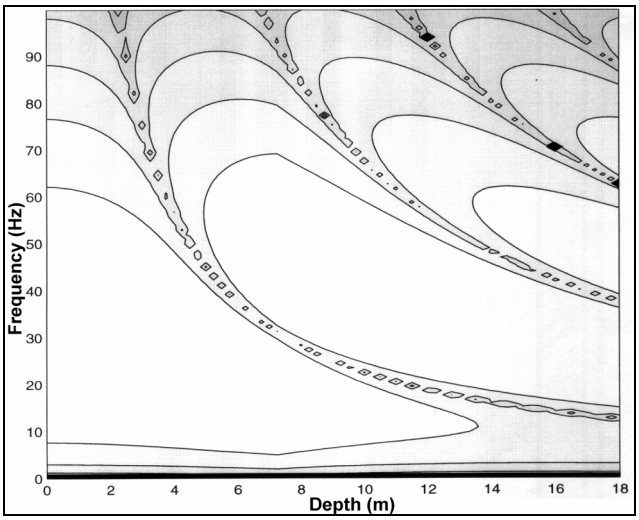


Figure 10. Expected receiver notching pattern for a constant V=900 m/s medium.

The contoured plot of Figure 11 simulates expected receiver notching patterns for converted waves in a linear V(z). In this plot, the dominant frequency of the Ricker wavelet is 12 Hertz, and the average velocity and gradient of the medium resemble near-surface shear-wave velocities of the Blackfoot area ($V_0$=150 m/s, $V_{18}$=400 m/s). There are up to six notches in the spectrum for typical converted-wave frequencies, which is more than appear in the compressional-wave simulations.



Contents

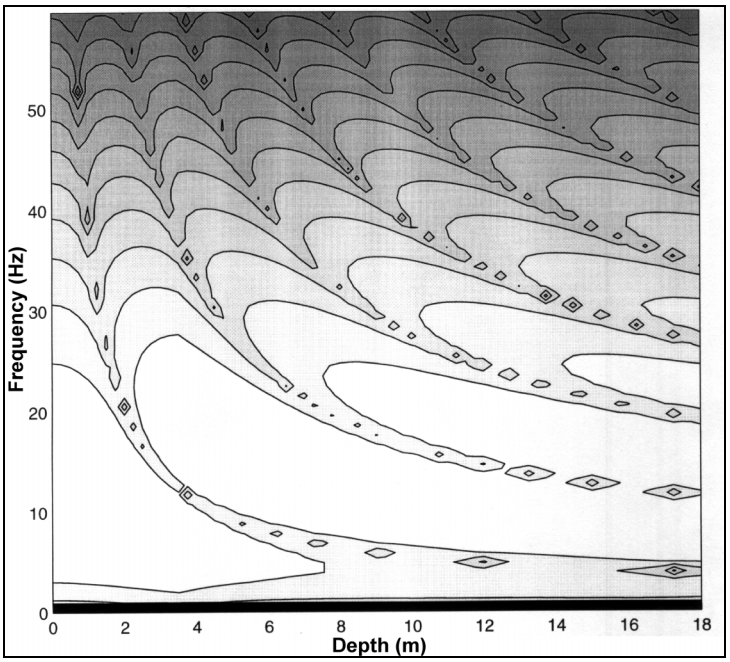


Figure 11. Expected receiver notching patterns for a simulated converted wave in a linear V(z): $V_0$=150 m/s, $V_{18}$=400 m/s.

The simulations indicate that in a linear V(z), some amount of receiver notching will occur for depths greater than one meter, and the notches will not be at a consistent frequency between different depths. The number of notches appearing is proportional to depth and inversely proportional to the average velocity and velocity gradient of the media. The notches will asymptotically approach zero frequency at a rate that is inversely proportional to the average velocity and velocity gradient of the medium.

## Wavelet Interference Effects on Amplitude

As demonstrated in Figure 6, interference between the incident and reflected wavelets may cause a significant reduction in recorded amplitudes. Figure 12 shows the maximum amplitude recorded at each geophone depth for the entire record for several velocity gradients. The data have been normalized so that the maximum amplitude of the incident wavelet is 1.00. Amplitudes at surface are 2.00 due to the free surface effect. In all cases, amplitudes decrease rapidly to about 27% of surface values, at a depth proportional to velocity gradient and average velocity of the media. Past this minimum, amplitudes recover gradually back to those of the incident wavelet at a rate inversely proportional to velocity gradient. For steep gradients and high velocities, amplitudes do not achieve that of the incident wavelet even at a depth of 18 meters.

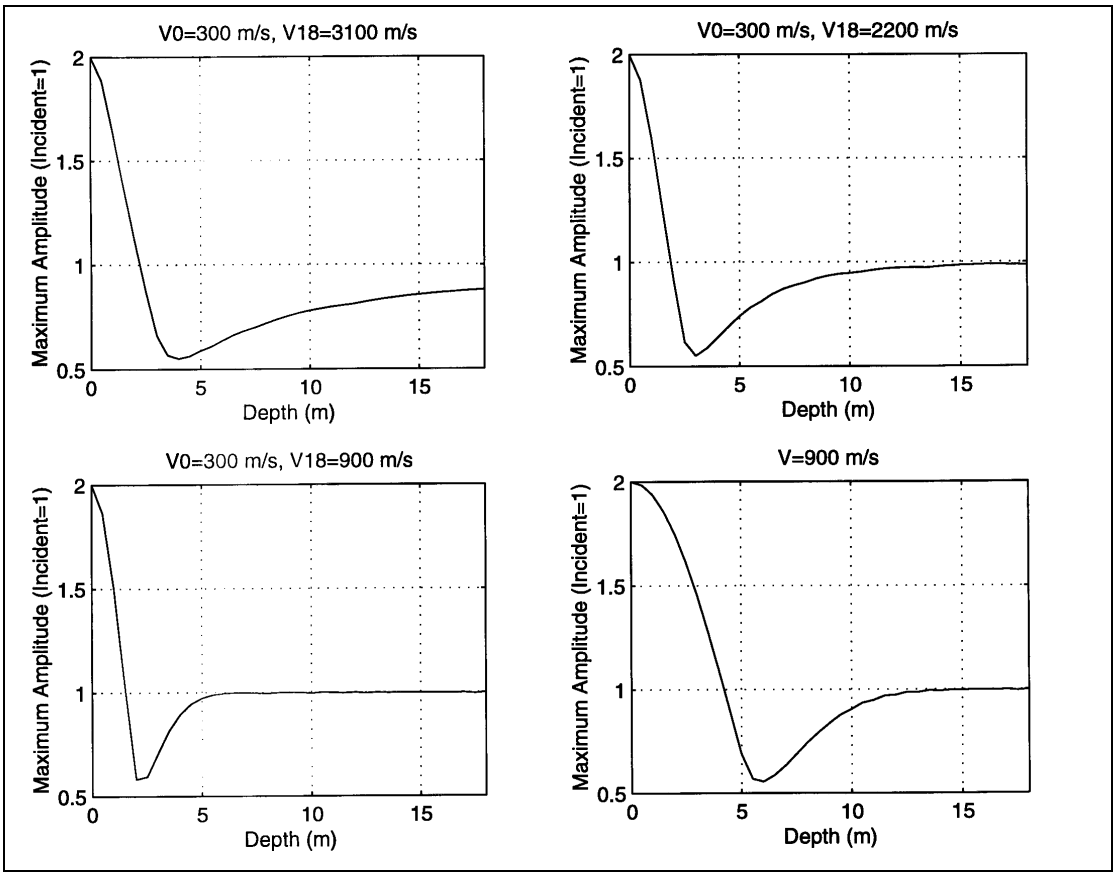


Figure 12. Maximum amplitude of the total wavefield at each geophone depth for four velocity gradients.

## Near-Surface Impedance Effects on Amplitude

The normal-incidence transmission coefficient T for a wave traveling from a medium of impedance $I_1$ ($=v_1\rho_1$) to a medium of impedance $I_2$ ($=v_2\rho_2$) is

$$T = \frac{2I_1}{I_2 + I_1}.$$

This is a good approximation for angles of incidence of up to 15° for most rock interfaces (Sheriff and Geldart, p. 76). Note that if $I_2<I_1$, then $T>1$; in other words, the amplitude of a wave increases when passing into a medium of lower impedance. The event conserves energy, as the transmission coefficient for energy is $(I_2/I_1)T^2$, which is one or less for all impedance contrasts. The above equation implies that a wave traveling in a medium of decreasing impedance (such as a reflection vertically ascending through the near surface) will experience increasing amplitude. To simulate this, a linear V(z) model from the receiver notch simulations was multiplied by a linear ρ(z) model to derive an I(z) impedance model. The density model is a linear gradient from $\rho_{18}$=2400 kg/m$^3$ (plausible for unweathered bedrock) to $\rho_0$=1200 kg/m$^3$ (perhaps representing dry clay that has been chemically weathered). The I(z) impedance model was divided into 18 discrete, equal steps, and the transmission coefficients were calculated at the boundary of each step using the above equation.



Contents

The amplitude of a wave in a given layer traveling vertically through the model is simply the product of the transmission coefficients of the boundaries the wave has passed through. Simply doubling the last calculated amplitude simulates the free surface effect.

The absolute amplitudes of the real buried geophone data are essentially arbitrary, so the synthetic amplitudes are all multiplied by a constant value to match the real data.

## COMPARISON TO BLACKFOOT III BURIED GEOPHONE DATA

Data from the Blackfoot III buried geophone experiment contained numerous noise sources (e.g. ground roll, refractions, 60 Hertz contamination) that were not included in the synthetic simulations. Therefore, to properly compare the real data to the simulations, the field data were passed through an f-k filter designed to reject ground roll and refracted energy. The filter effectively isolated the reflected data that were used for analysis. The filtering was performed in Promax and then the data were imported into Matlab for frequency analysis.

### Amplitudes

An amplitude-depth relationship was noted early on in the buried geophone data analysis. Figures 13 and 14 show semi-log plots of compressional- and converted-wave reflection average absolute amplitudes versus depth of receiver gathers, in a certain time window. Note that the geophones could not always be placed at the desired depth due to hole caving or when the shot hole augur encountered hard bedrock or boulders. The reflection amplitudes decrease with depth, a phenomenon observed previously for buried geophones (Houghton, 1940). Also plotted are the amplitudes for a simulated wavelet (scaled by a constant) travelling through an I(z) model as described in the previous section. Though the geophone reflection amplitudes exhibit some scatter, they have an overwhelming agreement to the impedance model amplitudes. No amplitude minimum can be seen in the data as predicted by wavelet interference simulations, although the six meter depth geophones recorded slightly lower P-wave amplitudes than expected from the impedance model. Whether this disagreement between the real and predicted reflection amplitudes is due to wavelet interference or discrepancies between the model and the true near surface cannot be said at this time.

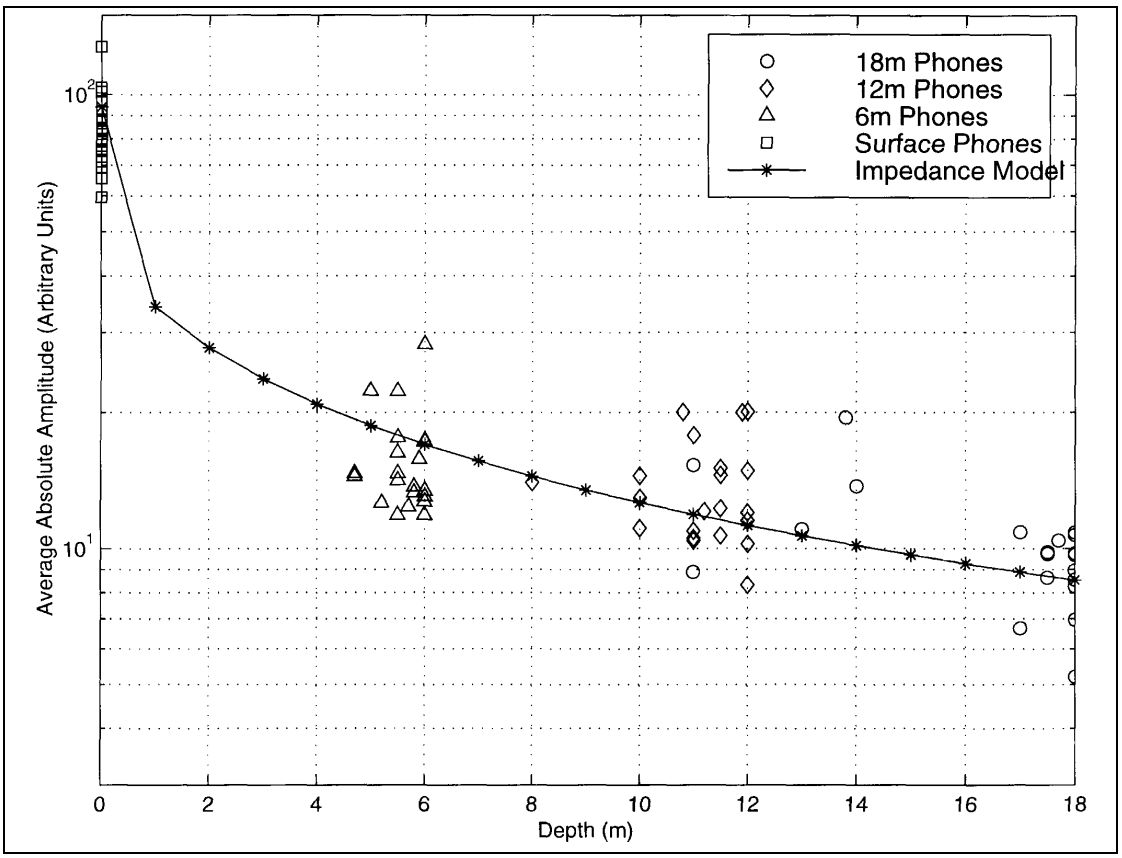


Figure 13. Actual and modeled reflection amplitudes for P-wave as recorded by buried geophones. Actual data points are the absolute amplitudes of P-P reflections between 900 and 2000 ms from the Blackfoot III buried geophone data. Data were f-k filtered to suppress ground roll and refracted energy prior to amplitude analysis. Modeled amplitudes are from an 18-step I(z) impedance model where $I(z)=V(z)\rho(z)$; $V_{18}$=3100 m/s, $V_0$=300 m/s, $\rho_{18}$=2400 kg/m$^3$, $\rho_0$=1200 kg/m$^3$.



Contents

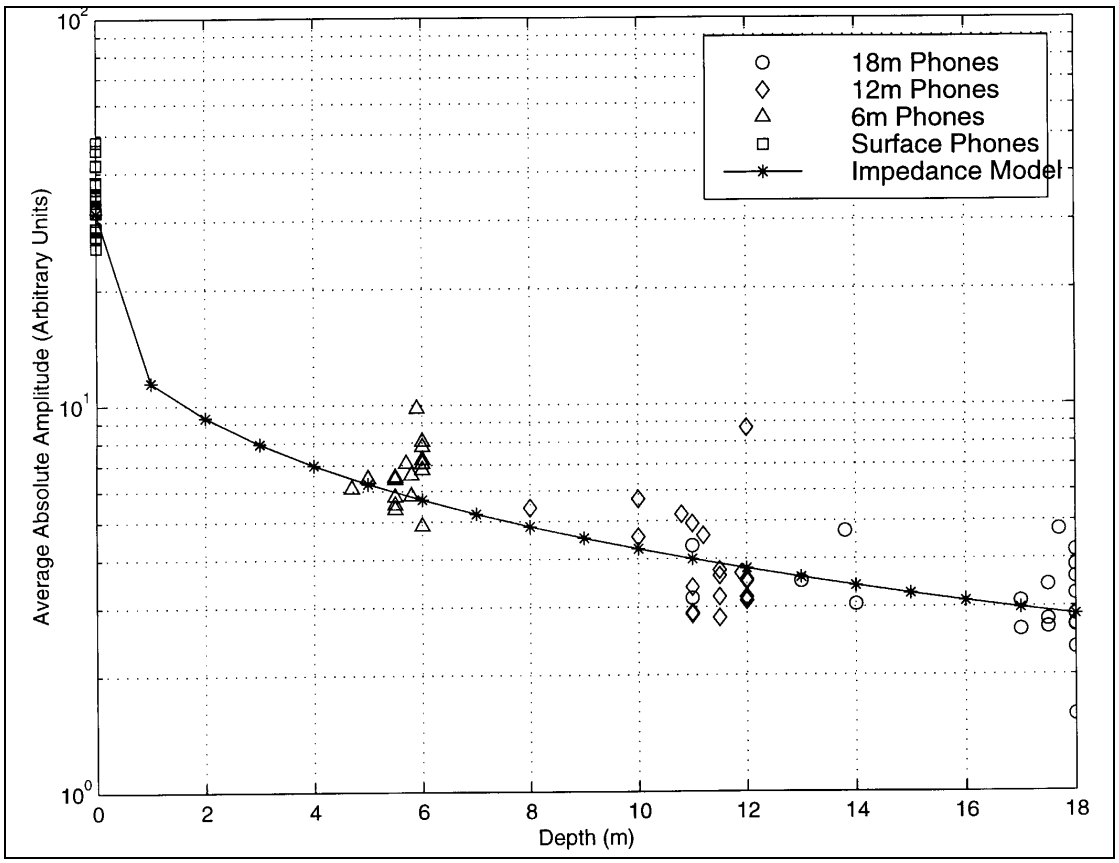


Figure 14. Same as Figure 13 for P-S reflections between 1400 and 2400 ms. Impedance model is based on linear $V_{18}$=1500 m/s, $V_0$=150 m/s, and linear $\rho_{18}$=2400 kg/m$^3$, $\rho_0$=1200 kg/m$^3$.

## Frequencies

The f-k filtered data from several buried geophone stations were analyzed for frequency content using Matlab software (Margrave, 1998). The analysis windows for frequency were the same as those used to analyze amplitudes (Figures 13 and 14). Figure 15 shows an example of the frequency spectra for converted-wave reflections for all depths of a certain buried geophone station. The spectra are rather noisy despite the f-k filtering. Many notches occur in the data that are present at all depths; the causes of these may include source ghosts, interbed multiples, near-surface reverberations and the earth's true reflectivity. This complicates the search for receiver notches as it is possible one may appear at a frequency that is already notched for a different reason. Also, regardless of its cause, a notch cannot extend to amplitudes below the base level of incoherent noise in the data, so they cannot be expected to be as large as those predicted by the synthetic analysis.

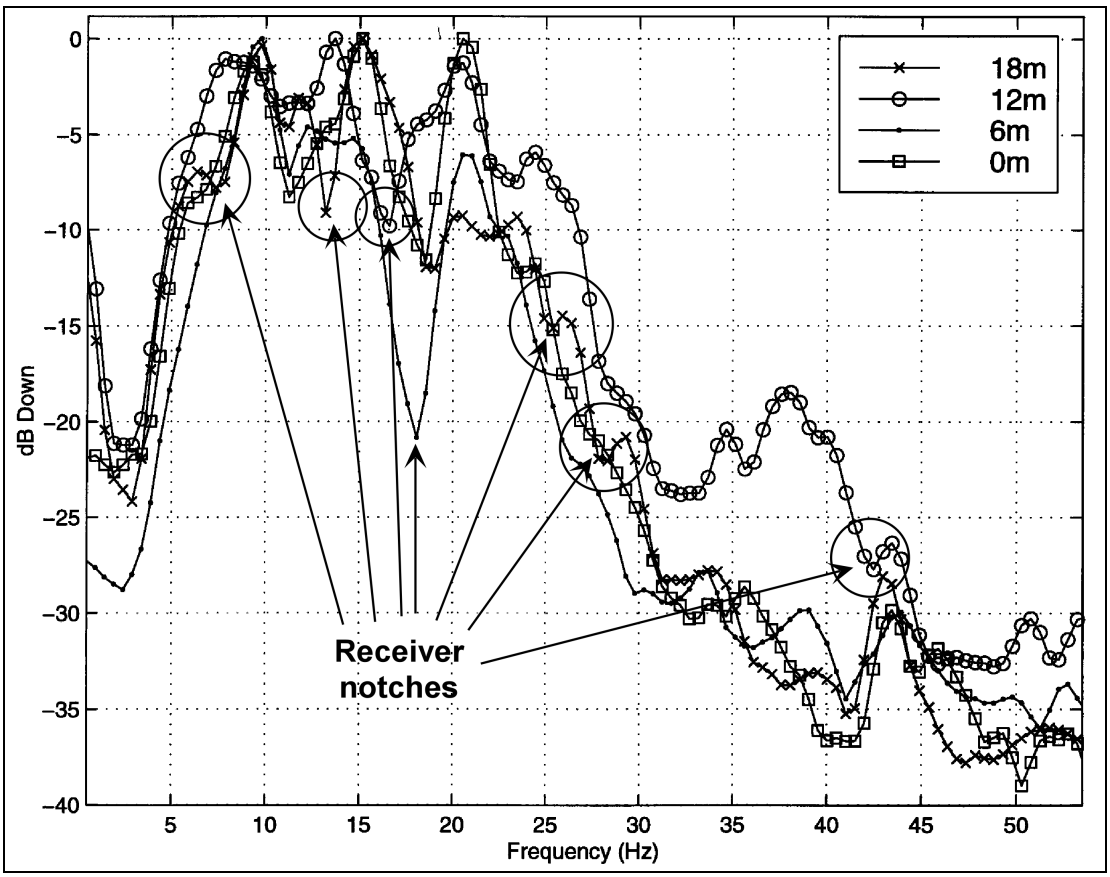


Figure 15. Frequency spectra for converted-wave reflections from the Blackfoot III buried geophone experiment. Arrows indicate possible receiver notches.

Nevertheless, there are several notches that appear at one depth but not at the others, indicated with arrows on Figure 15. One such notch at about 18-Hertz is quite pronounced; other notches are more subtle. The frequency spectrum from the 18 meter depth geophone contains more notches than the spectrum of the 12 meter geophone, which in turn contains more notches than the spectrum of the 6 meter geophone. This observation is consistent with the synthetic results. Other buried geophone stations show a similar pattern.

Figure 16 shows the amplitude spectra for all depths of geophone of compressional-wave reflections. There are fewer depth-dependent notches observable in the spectra (indicated with arrows) than was the case for the converted-wave data. This was observed to be true in general for the buried geophone data. In many cases, no convincing receiver notches could be found, indicating perhaps that in practice the receiver notches are too superimposed with signal and random noise to be readily identifiable.



Contents

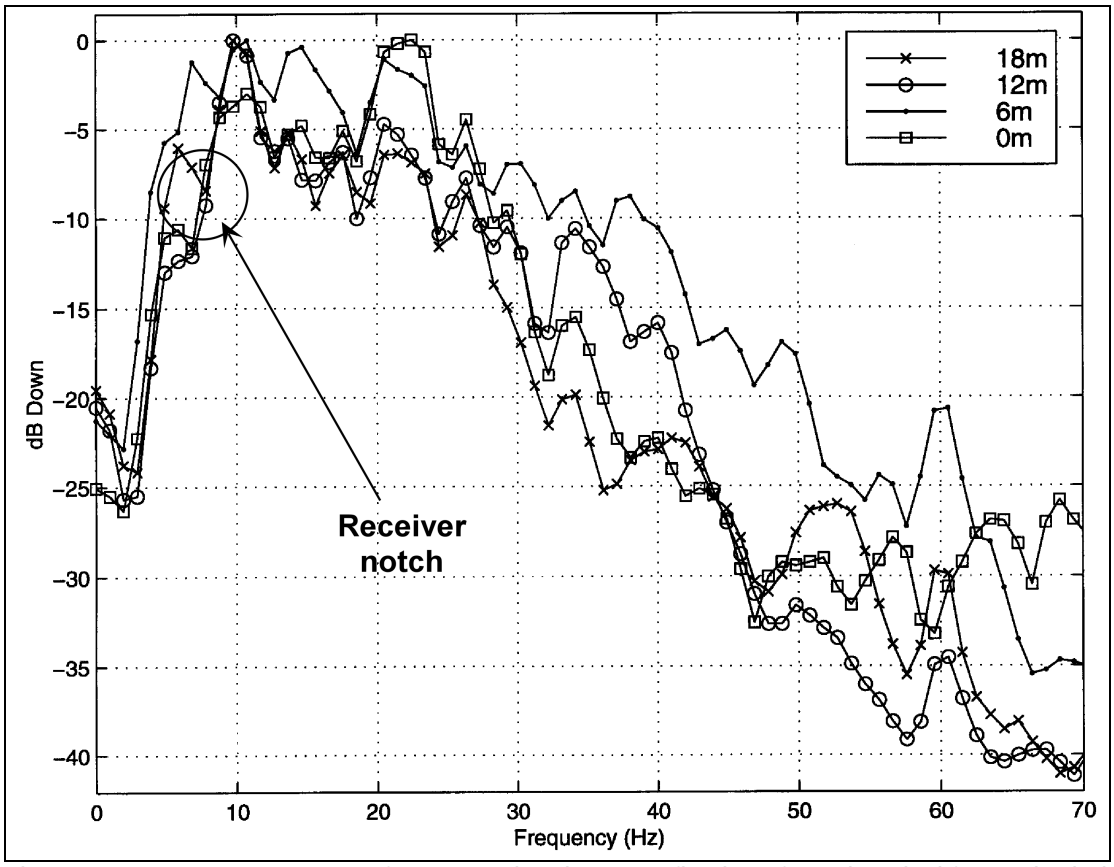


Figure 16. Frequency spectra of compressional-wave reflections from the Blackfoot III buried geophone experiment. A possible receiver notch is indicated.

As seismic velocities for unconsolidated material are known to be much higher for P-waves than S-waves, particularly below the water table (Lawton, 1990), the observed notching patterns are consistent with those predicted by the Ricker wavelet simulations.

## CONCLUSIONS

Wavelet interference simulations indicate that more receiver notches will occur in lower-velocity media with smaller velocity gradients. The frequency spectra of deeper geophones would be more notched than frequency spectra of shallower geophones. As predicted, the radial channel data contained more receiver notches than the vertical channel data. Many vertical channel receiver gathers did not contain clear examples of receiver notches, probably due to random noise and overprinting by notches from other causes.

Wavelet interference is also predicted to cause amplitudes to decrease to some minimum value at depth (proportional to average velocity and gradient) and then increase gradually. This was not observed in the real data. The impedance model predicted an overall decrease of reflection amplitude with depth, which matched the real data extremely well. This indicates that the near surface naturally amplifies reflections, as a result of its sharp impedance gradient, resulting in higher average absolute amplitudes in shallower geophones.

## RECOMMENDATIONS

Unlike marine surveys, near-surface complexity precludes determining an optimal depth at which to place geophones, other than the surface. Even where the near surface is relatively well known, the added consideration must be made of finding a depth that is free from receiver notches in the bandwidths of both compressional- and converted-wave reflections.

It is recommended that the near-surface models be modified to a "second approximation" of the true near surface. For P-waves, the velocities would increase in two large, discrete steps, representing the water table and the top of the bedrock. There would be only one step for the S-wave as they are relatively unaffected by the presence of the water table. Velocities at intermediate locations would have a gradual, linear taper.

## ACKNOWLEDGEMENTS

We thank the sponsors of CREWES for suggesting this work. Dr. Gary Margrave provided helpful input to this research, for which we are grateful.

## REFERENCES

Barr, F.J. and Sanders, J.I., 1989, Attenuation of water-column reverberations using pressure and velocity detectors in a water-bottom cable: Presented at the 59th Annual SEG Meeting.

Cieslewicz, D. and Lawton, D.C., 1998b, Results from the Blackfoot III buried geophone experiment: CREWES Research Report **8**, Ch. 2

Cieslewicz, D. and Lawton, D.C., 1998a, A three-component field study of the low-velocity layer: Abstracts from the CSEG Annual General Meeting, p. 217-220.

Houghton, H.M. 1940. Change of reflection amplitude and character with geophone depth: Geophysics, **5**, 169-175.

Lawton, D.C., 1990. A 9-component refraction seismic experiment: Canadian Journal of Exploration Geophysics, **26**, 7-16.

Margrave, G.F., 1998, unpublished: Seismic signal band estimation using f-x spectra.

Miller, D.M. and Xia, J, 1998, Large near-surface velocity gradients on shallow seismic reflection data: Geophysics, **63**, 1348-1356

Sheriff, R.E. and Geldart, L.P., 1995, *Exploration Seismology*, 2nd ed. Cambridge: Cambridge University Press

Waters, K.H. 1987. *Reflection Seismology*, 3rd. Ed. New York: John Wiley